AD_____

Award Number: W81XWH-11-1-0248

TITLE: Echo-Planar Imaging-Based, J-Resolved Spectroscopic Imaging for Improved Metabolite Detection in Prostate Cancer

PRINCIPAL INVESTIGATOR: Michael Albert Thomas Ph.D.

CONTRACTING ORGANIZATION:
The Regents of the University of California
Los Angeles, CA 90024-1406

REPORT DATE: October 2015

TYPE OF REPORT: Annual

PREPARED FOR: U.S. Army Medical Research and Materiel Command
Fort Detrick, Maryland 21702-5012

REPORT DOCUMENTATION PAGE

Form Approved
OMB No. 0704-0188

1. REPORT DATE	2. REPORT TYPE	3. DATES COVERED
October 2015	Annual	30 Sep 2014 - 29 Sep 2015

4. TITLE AND SUBTITLE

Echo-Planar Imaging-Based, J-Resolved Spectroscopic Imaging for Improved Metabolite Detection in Prostate Cancer

5a. CONTRACT NUMBER

5b. GRANT NUMBER
W81XWH-11-1-0248

5c. PROGRAM ELEMENT NUMBER

6. AUTHOR(S)
Michael Albert Thomas Ph.D.

E-Mail: athomas@mednet.ucla.edu

5d. PROJECT NUMBER

5e. TASK NUMBER

5f. WORK UNIT NUMBER

7. PERFORMING ORGANIZATION NAME(S) AND ADDRESS(ES) AND ADDRESS(ES)
The Regents of the University of California The OCGA
University of California, Los Angeles 11000 Kinross Ave.
Kim Duiker, Assistant Director Suite#211
Los Angeles, CA 90095

8. PERFORMING ORGANIZATION REPORT NUMBER

9. SPONSORING / MONITORING AGENCY NAME(S) AND ADDRESS(ES)
U.S. Army Medical Research and Materiel Command
Fort Detrick, Maryland 21702-5012

10. SPONSOR/MONITOR'S ACRONYM(S)

11. SPONSOR/MONITOR'S REPORT NUMBER(S)

12. DISTRIBUTION / AVAILABILITY STATEMENT
Approved for Public Release; Distribution Unlimited

13. SUPPLEMENTARY NOTES

14. ABSTRACT
Purpose: 1) To implement an echo-planar imaging (EPI)-based 2D J-resolved spectroscopy on a 3T MRI/MRS scanner;2) To evaluate the multi-voxel 2D J-resolved echo-planar spectroscopic imaging (EP-JRESI) in malignant PCa patients, benign prostatic hyperplasia (BPH) patients and healthy prostates. 3) To develop and further optimize the ProFit algorithm to post-process the multi-dimensional MRS data from different prostate pathologies.
Scope: Improved cancer detection (specificity) in differentiating malignant from benign prostate cancer will be achieved using a novel four-dimensional (4D) EP-JRESI. Improved spectroscopic imaging techniques will enable unambiguous detection of metabolites and the lipids in situ, which could potentially complement the existing diagnostic modalities commonly used in prostate cancer.
Progress and Major Findings: After successful implementation of the 4D EP-JRESI sequence on a 3T MRI scanner, the 4D EP-JRESI data were recorded in several patients and healthy males during the first three years. Thirteen more male subjects (10 patients and 3 healthy) were investigated using endorectal as well as external MRI coils and the findings are reproducible with that obtained in the past years. A peer-reviewed manuscript was published in a leading MR journal in 2015.

15. SUBJECT TERMS: Digital Rectal Examination, prostate specific antigen, Four Dimensional (4D) Echo-Planar J-Resolved Spectroscopic Imaging (EP-JRESI); Citrate, Choline, Creatine, Spermine, 3Tesla MRI scanner, Endo-rectal MR coil, WET Water Suppression, prostate cancer (PCa), benign prostatic hyperplasia (BPH), prior-knowledge fitting

16. SECURITY CLASSIFICATION OF:			17. LIMITATION OF ABSTRACT	18. NUMBER OF PAGES	19a. NAME OF RESPONSIBLE PERSON
a. REPORT	b. ABSTRACT	c. THIS PAGE			USAMRMC
U	U	U	UU	**18**	19b. TELEPHONE NUMBER *(include area code)*

Table of Contents

Page

Introduction: Prostate cancer (PCa) is the most common cancer in men in several countries, with the American Cancer Society (ACS) estimating 241,740 new cases of PCa to be diagnosed and deaths of 28,170 men of PCa (1). Due to its prevalence in the male population as well as its unpredictable clinical course, early detection and diagnosis have become a priority for many health care professionals. Another method for staging prostate cancer is through imaging techniques including ultrasound, computed tomography (CT), and magnetic resonance imaging (MRI) with or without the help of dynamic contrast enhancement modeling (DCE-MRI), diffusion weighted imaging (DWI), and magnetic resonance spectroscopy (MRS) (2-5). MRS is a powerful tool for exploring the cellular chemistry of human tissues (3,5,6-11). There is a growing body of evidence that 1H MRS may contribute to the clinical evaluation of prostate cancer and also for evaluating the metabolic alterations due to therapy. There have been no reports on combining two spectral dimensions with two-dimensional (2D) or three dimensional (3D) spatial encoding applicable to prostate cancer. Acceleration of magnetic resonance spectroscopic imaging (MRSI) has been demonstrated using echo-planar imaging techniques (12-13). Recently, Schulte et al. have successfully developed an algorithm called prior-knowledge fitting (ProFit) to quantify metabolite concentrations using the JPRESS spectra recorded using a Philips 3T MRI scanner (14). It was demonstrated that metabolite quantitation of JPRESS spectra with ProFit was accurate, robust and yielding generally consistent results, both *in vivo* and *in vitro*. Their results suggest that the number of quantifiable prostate metabolites can be increased from 3-4 with 1D PRESS/LC-Model to more than 10 with JPRESS/ProFit (15-16).

Body:

i) Proposed Task 1 (Months 1-6)*: To implement a multi-voxel based extension of the JPRESS sequence, in which two spectral encodings will be combined with two spatial encodings using the new Siemens VB17a platform. This four-dimensional (4D) data acquisition scheme will be accomplished utilizing the EPI approach that is commonly used for spatial encoding in MRI.*

Completed and Reported in the 1st year Annual Report.

ii) ***Proposed Task 2:*** *To evaluate the EPI-based JPRESS using a prostate phantom containing several metabolites which have been reported in prostate tissues, and to optimize the EP-JJRESI sequence and other acquisition parameters using the phantom (**Months 6-12**).*

Completed and Reported in the 1st year Annual Report.

iv) Proposed Task 3: *To record the 4D EP-JRESI spectra in the peripheral, central and transition zones of healthy prostates. (**Months 6-18**).*

Five more healthy males have been investigated.

Proposed Task 4: *To develop, evaluate and optimize the prior-knowledge basis set spectra using the GAMMA-simulation and prostate phantom solutions as prior knowledge for the multi-voxel based JPRESS spectra recorded using the 3T MRI scanner (**Months 6-12**).*

Accomplished during September 29, 2011-October 28 2012:

***Proposed Task* 5:** To record the multi-voxel-based 2D spectra in the peripheral, central and transition zones of patients with BPH and malignant prostate cancer. The prostate metabolite concentrations calculated using the ProFit algorithm prepared for the multi-voxel data will be compared with LC-Model processed 1D spectral based MRSI data (**Months 18-48**).

Accomplished during October 29, 2014-October 28 2015: Ten malignant prostate cancer patients and three healthy males were investigated during the current year. The 4D EP-JRESI data were recorded using the following parameters: TR/TE=1.5s/30ms, 2 averages, 512 t_2, oversampled $32k_x$, 64 increments along the indirect spectral (t_1) and 16 spatial k_y dimensions; the endorectal "receive" coil. The oversampled $32k_x$ were processed to normal $16k_x$ points. First, the 4D NUS EP-JRESI data was acquired in a 71 year old PCa patient; In our recent publication, we had included twenty two PCa patients with a mean age of 63.8 years (range: 46–79 years) who subsequently underwent radical prostatectomy. Patients' Gleason scores varied between 6 and 9. Prostate-specific antigen (PSA) levels varied from 0.7 to 22.8 ng/mL (mean of 6.23 ng/mL).

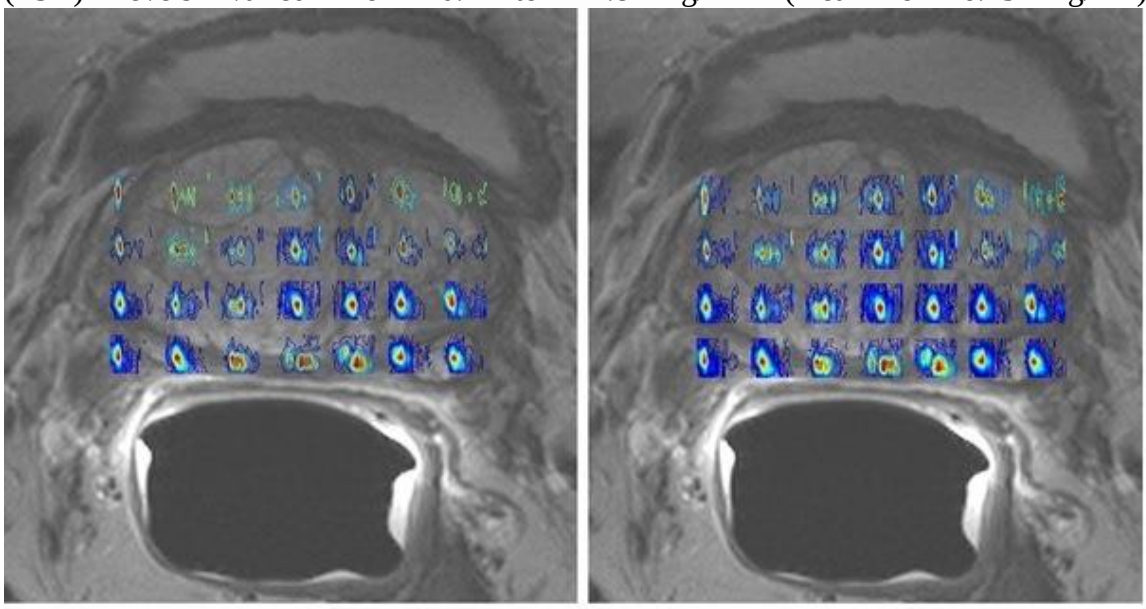

Figure 1. Spatial maps of (Ch +Cr) for TV (A) and MaxEnt (B) non-linear reconstruction methods of the 4D EP-JRESI data recorded in a 74 year old PCa patient. The EP-JRESI was overlaid on top of the T_2 weighted MRI

We were able to reproduce the above mentioned findings in more patients with known GS, and also, in remaining four patients whose histology findings were not known. 2D peak (cross and diagonal) volumes were defined by the operator in the frequency domain 2D JPRESS data for this pilot analysis. Two different non-linear reconstruction methods such as maximum entropy (MaxEnt) and total variation (TV). As

evident in Fig.2, selected ratios showed significant changes ($p<0.05$); however, this outcome from a small group of PCa patients

Fig.2. Metabolite ratios of Cit, Spm, mI and Glx in cancer and non-cancer locations processed by non-linear reconstruction methods using TV and MaxEnt.

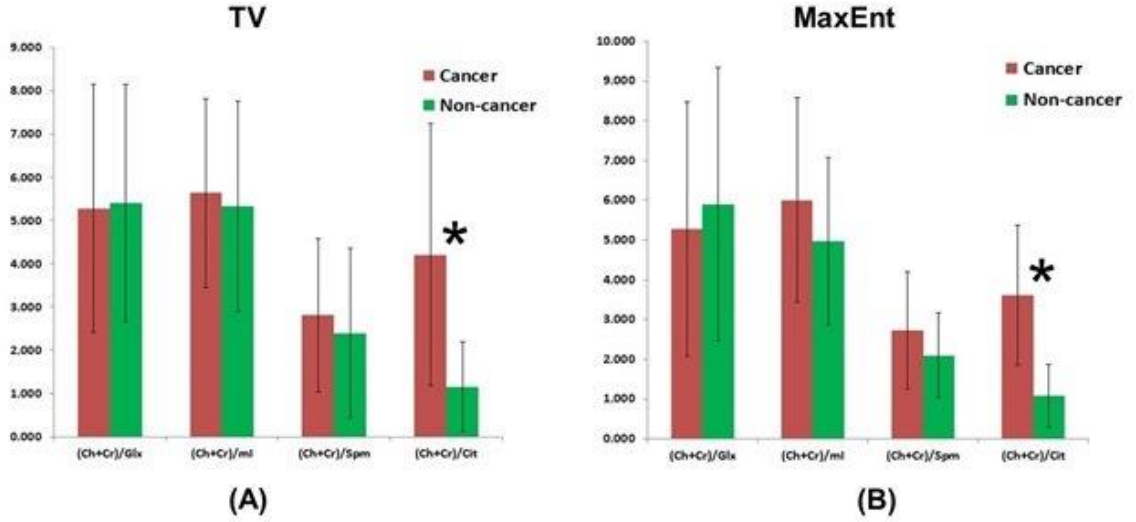

needs to be treated with caution showing a necessity for further research using larger patient cohorts.

Key Research Accomplishments

- Continued evaluation of the 4D EP-JRESI sequence in 10 malignant prostate cancer patients and three healthy male subjects.
- We have made further progress on compressed sensing reconstruction of the non-uniformly undersampled 4D EP-JRESI sequence using different reconstruction methods such as maximum entropy, total variation (TV), etc . This will facilitate shortening the endorectal spectral acquisition and reducing the patient inconvenience during the scan. A peer-reviewed manuscript was published recently in the journal of 'NMR in Biomedicine'.
- Using the preliminary results obtained using this IDEA grant, we had submitted a NIH R01 grant application submission entitled "Fast J-resolved Prostate MR Spectroscopic Imaging and Non-linear Reconstruction" was resubmitted on February 5, 2015 and we plan to resubmit this grant to NIH.

Reportable Outcomes:

A. Peer-reviewed Publications:

1. Nagarajan R, Iqbal Z, Burns B, et al. Accelerated Echo Planar J-Resolved Spectroscopic Imaging in Prostate Cancer: Nonlinear Reconstruction Using Total Variation And Maximum Entropy. NMR in Biomedicine 2015; 28: 1366–1373.

B. Presentations: During the 4th year, two abstracts were presented: (i) first at the 23rd International Society of Magnetic Resonance in Medicine (ISMRM), Toronto, Canada, May 30-June 5, 2015: the abstract entitled "Semi-Laser 5D Echo-Planar J-Resolved

Spectroscopic Imaging: Pilot Validation in Prostate Cancer." (ePoster presentation), #2020; the 2nd abstract entitled "How Accurately Multiparametric MRI Detect Prostate Cancer?" (eposter), # LL-PHE118;.

C. Books: A book chapter including some prostate data was published in the following chapter: Huda A, Nagarajan R, Furuyama J and Thomas MA. In Vivo Two-Dimensional Magnetic Resonance Spectroscopy "Comprehensive Biomedical Physics" Elsevier Publishers, 2014, Pp 359-77.

Conclusions: After successfully implementing the 4D EP-JRESI scanning protocol on the 3T MRI scanner and testing it in healthy controls and patients during the earlier 3 years, 13 more subjects have been investigated in the 4th year. We will continue to recruit 10 malignant and benign prostate cancer patients, and 5 healthy male subjects during the next year (2^{nd} no-cost time extension). Two new manuscripts and few conference abstracts will be prepared to present the summary of findings.

References

1) Dall'era MA, Cooperberg MR, Chan JM, *et al*. Active surveillance for early-stage prostate cancer: review. Cancer. 2008 Apr 15;112(8):1650-9. **PMID: 18306379**
2) McNeal JE. Normal histology of the prostate. Am J Surg Pathol 1988;12:619-633. **PMID: 2456702**
3) Weinreb JC, Blume JD, Coakley FV, et al. Prostate cancer: sextant localization at MR imaging and MR spectroscopic imaging before prostatectomy--results of ACRIN prospective multi-institutional clinicopathologic study. Radiology. 2009 Apr;251(1):122-33. **PMID: 19332850**
4) Jacobs MA, Ouwerkerk R, Petrowski K and Macura KJ. Diffusion-weighted imaging with apparent diffusion coefficient mapping and spectroscopy in prostate cancer. Top Magn Reson Imaging. 2008;19:261-72 **PMID:19512848**
5) Scheenen TW, Heijmink SW, Roell SA, et al. Three-dimensional proton MR Spectroscopy of human prostate at 3T without endorectal coil: feasibility. Radiology 2007;245:507-16. **PMID: 17848681**
6) Thomas MA, Narayan P, Kurhanewicz J, Jajodia P, Weiner MW. 1H MR spectroscopy of normal and malignant human prostates in vivo. J Magn Reson 1990; 87:610–619. **PMID:N/A**
7) Thomas MA, Narayan P, Kurhanewicz J, *et al*. Detection of phosphorus metabolites in human prostates with a transrectal ^{31}P NMR probe. J Magn Reson 1992; 99: 377-386. **PMID: N/A**
8) Narayan P, Kurhanewicz J. Magnetic Resonance spectroscopy in prostate disease: diagnostic possibilities and future developments. Prostate 1992; Suppl 4: 43-50. **PMID: 1374177**
9) van der Graaf M, Schipper RG, Oosterhof GO, J.A. Schalken, AA. Proton MR spectroscopy of prostatic tissue focused on the detection of spermine, a possible biomarker of malignant behavior in prostate cancer. MAGMA 2000; 10(3):153-9. **PMID: 10873205**

10) Jordan KW and Cheng LL. NMR-based metabolomics approach to target biomarkers for human prostate cancer. Expert Rev Proteomics 2007;4:389-400. **PMID: 17552923**
11) Kurhanewicz J, Swanson MG, Nelson SJ, and Vigneron DB. Combined magnetic resonance imaging and spectroscopic imaging approach to molecular imaging of prostate cancer. J Magn Reson Imaging 2002;16(4):451-463. **PMID: 12353259**
12) Mansfield P. Spatial mapping of the chemical shift in NMR. Magn Reson Med 1984; 1: 370 – 386. PMID:6571566
13) Posse S, Otazo R, Caprihan A, et al. Proton echo-planar spectroscopic imaging of J-coupled resonances in human brain at 3 and 4 Tesla. Magn Reson Med 2007; 58(2): 236-44. PMID: 17610279
14) Schulte RF and Boesiger P. ProFit: two-dimensional prior-knowledge fitting of J-resolved spectra. NMR Biomed 2006;19:255-263. **PMID: 16541464**
15) Lange T, Schulte RF and Boesiger P. Quantitative J-resolved prostate spectroscopy using two-dimensional prior-knowledge fitting. Magn Reson Med 2008;59:966-972. PMID: 18429013
16) Thomas MA, Lange T, Velan SS, et al. Two-dimensional MR Spectroscopy of healthy and cancerous prostates in vivo. Magn Reson Mater Phy (MAGMA) 2008;21(6):443-58. **PMID**: **18633659**
17) Wright A, Tessem MB, Bertilsson H, et al. Quantitative 1H HR-MAS using LC Model shows glutamate, choline, glycerylphosphocholine, and glucose as biomarkers of prostate. Proc Intl Soc Magn Reson Med 2012;20:2975. **PMID: N/A**
18) Stenman K, Hauksson JB, Grobner G, et al. Detection of polyunsaturated omega-6 fatty acid in human malignant prostate tissue by 1D and 2D high resolution magic angle spinning NMR spectroscopy. MAGMA 2009;22:327-31 **PMID: 19921294.**

Appendix:

1. Nagarajan R, Iqbal Z, Burns B, et al. Accelerated echoplanar J-resolved spectroscopic imaging in prostate cancer: a pilot validation of non-linear reconstruction using total variation and maximum entropy. NMR Biomed. 2015 Nov;28(11):1366-73.
2. Iqbal Z, Wilson N, Nagarajan R, et al. Semi-Laser 5D Echo-Planar J-Resolved Spectroscopic Imaging: Pilot Validation in Prostate Cancer. Abstract presented at the International Society for Magnetic Resonance in Medicine – 23rd Scientific Meeting 2015 (Toronto, Canada). Proceedings of the International Society for Magnetic Resonance in Medicine, Abstract, 2020, 2015.
3. Nagarajan R, Margolis DJ, Raman SS, et al. How Accurately Multiparametric MRI Detect Prostate Cancer?. Abstract presented at the Radiological Society of Northern America (RSNA) – 100th Scientific Meeting 2014 (Chicago, USA). Proceedings of the Radiological Society of Northern America. 2014, published online at www.rsna2014.rsna.org, Abstract LL-PHE118, 2014.

Research article

NMR IN BIOMEDICINE

Received: 10 September 2014, Revised: 16 July 2015, Accepted: 17 July 2015, Published online in Wiley Online Library: 7 September 2015

(wileyonlinelibrary.com) DOI: 10.1002/nbm.3373

Accelerated echo planar *J*-resolved spectroscopic imaging in prostate cancer: a pilot validation of non-linear reconstruction using total variation and maximum entropy

Rajakumar Nagarajan[a], Zohaib Iqbal[a], Brian Burns[a], Neil E. Wilson[a], Manoj K. Sarma[a], Daniel A. Margolis[a], Robert E. Reiter[b], Steven S. Raman[a] and M. Albert Thomas[a]*

The overlap of metabolites is a major limitation in one-dimensional (1D) spectral-based single-voxel MRS and multivoxel-based MRSI. By combining echo planar spectroscopic imaging (EPSI) with a two-dimensional (2D) *J*-resolved spectroscopic (JPRESS) sequence, 2D spectra can be recorded in multiple locations in a single slice of prostate using four-dimensional (4D) echo planar *J*-resolved spectroscopic imaging (EP-JRESI). The goal of the present work was to validate two different non-linear reconstruction methods independently using compressed sensing-based 4D EP-JRESI in prostate cancer (PCa): maximum entropy (MaxEnt) and total variation (TV). Twenty-two patients with PCa with a mean age of 63.8 years (range, 46–79 years) were investigated in this study. A 4D non-uniformly undersampled (NUS) EP-JRESI sequence was implemented on a Siemens 3-T MRI scanner. The NUS data were reconstructed using two non-linear reconstruction methods, namely MaxEnt and TV. Using both TV and MaxEnt reconstruction methods, the following observations were made in cancerous compared with non-cancerous locations: (i) higher mean (choline + creatine)/citrate metabolite ratios; (ii) increased levels of (choline + creatine)/spermine and (choline + creatine)/myo-inositol; and (iii) decreased levels of (choline + creatine)/(glutamine + glutamate). We have shown that it is possible to accelerate the 4D EP-JRESI sequence by four times and that the data can be reliably reconstructed using the TV and MaxEnt methods. The total acquisition duration was less than 13 min and we were able to detect and quantify several metabolites. Copyright © 2015 John Wiley & Sons, Ltd.

Keywords: MRS; prostate cancer; 4D EP-JRESI; citrate; myo-inositol; Glx; echo planar spectroscopic imaging

INTRODUCTION

Prostate cancer (PCa) is the most commonly diagnosed non-cutaneous malignancy in the USA and is the second leading cause of cancer-related death in men (1). One in six men will be diagnosed with PCa during their lifetime, but only one in 36 will die of this disease. Currently, the annual prostate-specific antigen (PSA) test and digital rectal examination (DRE) are routinely performed (2) for screening. The PSA screening test measures the serum level of PSA in blood samples. However, it is a controversial test because 65–75% of PSA screening gives false-positive results leading to overdiagnosis (3). The use of systematic transrectal biopsy can miss significant cancer lesions because of random sampling error (4) and the observation that one-third of significant tumors lie in the anterior part of the gland, based on studies of radical prostatectomy specimens (5). Hence, there is an immediate need for early, yet accurate, detection of PCa to improve disease outcomes.

^{1}H MRS enables the detection of a range of biochemicals in the prostate by making use of the proton signals in these molecules. The detection of biochemicals *in vivo* is limited to concentrations of more than 0.5–1 mM. Signals of citrate (Cit), creatine (Cr), choline (Ch) and spermine (Spm) can be detected throughout the prostate, with increased levels of Ch and decreased levels of Cit being indicative of cancer (6–8).

* *Correspondence to: M. A. Thomas, Radiological Sciences, David Geffen School of Medicine at UCLA, Los Angeles, 90095 CA, USA.*
E-mail: athomas@mednet.ucla.edu

a *R. Nagarajan, Z. Iqbal, B. Burns, N. E. Wilson, M. K. Sarma, D. A. Margolis, S. S. Raman, M. A. Thomas*
Radiological Sciences, University of California Los Angeles, Los Angeles, CA, USA

b *R. E. Reiter*
Urology, University of California Los Angeles, Los Angeles, CA, USA

Abbreviations used: *1D, one-dimensional; 2D, two-dimensional; 3D, three-dimensional; 4D, four-dimensional; AUC, area under the curve; Ch, choline; Cit, citrate; Cr, creatine; DRE, digital rectal examination; EP-JRESI, echo planar J-resolved spectroscopic imaging; EPSI, echo planar spectroscopic imaging; Gln, glutamine; Glu, glutamate; Glx, glutamine + glutamate; JPRESS, J-resolved spectroscopy/spectroscopic; MaxEnt, maximum entropy; mI, myo-inositol; NPV, negative predictive value; NUS, non-uniform undersampling/non-uniformly undersampled; NWS, non-water-suppressed; PCa, prostate cancer; PPV, positive predictive value; PSA, prostate-specific antigen; PZ, peripheral zone; RF, radiofrequency; ROC, receiver operating characteristic; SNR, signal-to-noise ratio; Spm, spermine; TV, total variation; T2W, T_2-weighted; VOI, volume of interest; WS, water-suppressed.*

Current limitations of single-voxel-based MRS and MRSI in the prostate are caused by the overlap of metabolite resonances, allowing the quantification of only a few metabolites (Cit, Ch, Cr and Spm) and the use of long TEs. The conventional MRSI technique can be accelerated by echo planar spectroscopic imaging (EPSI) (9–13). EPSI speeds up MRSI using an echo planar readout of one spectral and one spatial dimension, thereby achieving an acceleration factor equal to the number of points along one of the spatial dimensions. For example, a two-dimensional (2D) spatial matrix array (16 × 16) would be acquired 16 times faster with EPSI than with conventional MRSI. However, the acceleration may be at the cost of the signal-to-noise ratio (SNR) (11) and the spectra could be affected by Nyquist ghost artifacts (14).

A single-voxel-based 2D J-resolved spectroscopic (JPRESS) sequence has been evaluated in PCa, and has shown improved spectral dispersion because of the added spectral dimension (15,16). New computational methods have made compressed sensing feasible to accelerate MRI by exploiting the sparsity of the images in a known transform domain to reconstruct non-uniformly undersampled (NUS) *k*-space data (17). For further acceleration, the application of compressed sensing for MRSI is apt, exploiting sparsity in multiple dimensions of frequency and space in transform domains of wavelets and total variation (TV) (18–20). By combining EPSI with JPRESS, 2D spectra can be recorded in multiple locations in the prostate using four-dimensional (4D) echo planar *J*-resolved spectroscopic imaging (EP-JRESI), which combines two spectral with two spatial dimensions. A pilot feasibility has been demonstrated recently to map metabolites in the healthy human prostate and brain (21,22).

Maximum entropy (MaxEnt) reconstruction finds the spectrum that maximizes entropy whilst maintaining consistency with the measured data. MaxEnt reconstruction is an alternative non-linear reconstruction technique to compressed sensing. MaxEnt has been successfully used to reconstruct undersampled images in astronomy and multidimensional spectra in NMR (23–25), but has not been applied to the spatial–spectral domain (k_y–t_1) of 4D EP-JRESI of PCa. MaxEnt and TV algorithms have been used to reconstruct the NUS indirect spectral and spatial dimensions (21,26).

The TV algorithm was first proposed by Rudin *et al.* (27) for image denoising and, since then, has been successfully used for image restoration. In the TV algorithm, an objective function using the TV norm is minimized subject to a data fidelity term posed by the acquired projection data. Minimization of the image gradient essentially suppresses those high spatial frequency parts, such as streaking artifacts and noise, in the reconstructed images.

The goal of the present work was to validate the MaxEnt and TV non-linear reconstruction algorithms separately in patients with PCa using compressed sensing-based 4D EP-JRESI data.

MATERIALS AND METHODS

Patients

Between March 2012 and May 2013, twenty-two patients with PCa with a mean age of 63.8 years (range, 46–79 years), who subsequently underwent radical prostatectomy, were selected for the study. The patients' Gleason scores varied between 6 and 9. Their PSA levels varied from 0.7 to 22.8 ng/mL (mean, 6.23 ng/mL). These patients were scanned using a 3-T Siemens (Siemens Medical Solutions, Erlangen, Germany) MRI scanner with an endorectal 'receive' coil. The protocol combining MRI and MRS was performed at least 8 weeks after transrectal ultrasound-guided sextant biopsy. The entire protocol was approved by the Institutional Review Board, and informed consent was obtained from each patient. PCa was histopathologically confirmed after radical prostatectomy. The voxels covering the tumorous lesions from the peripheral zone (PZ) were selected and indicated as tumor voxels, which was confirmed by the pathology report. After reconstruction, the EP-JRESI data were overlaid onto MRI images.

MRI and MRSI

A body matrix phased-array coil assembly, combined with an endorectal coil, was used in the 'receive' mode, whereas a quadrature body 'transmit' coil was used. All patients were imaged in the supine (feet-first) position. Axial images were oriented to be perpendicular to the long axis of the prostate, which was guided by the sagittal images. Axial, coronal and sagittal T_2-weighted (T_2W) turbo spin echo images were recorded using the following parameters: TR/TE = 3850–4200 ms/96–101 ms; slice thickness, 3 mm; field of view, 20 × 20 cm^2; echo train length, 13; data matrix, 320 × 256.

A compressed sensing-based 4D EP-JRESI sequence was validated on the 3-T MRI scanner and the volume of interest (VOI) was localized using three slice-selective radiofrequency (RF) pulses (90°–180°–180°) (Fig. 1). The total time for the acquisition of a fully sampled 4D EP-JRESI scan (TR = 1.5 s, 16k_y × 16k_x, 64–100t_1, 512t_2) can be more than 25 min. The parameters for EP-JRESI were as follows: TR/TE/Avg = 1500 ms/30 ms/2; 16 phase-encoding steps; 512 complex points with an F_2 bandwidth of 1190 Hz along the detected dimension. For the second dimension (F_1), 64 increments with bandwidths of 1000 Hz were used. The in-plane spatial resolution and slice thickness were 1 × 1 cm^2 and 1 cm, respectively. As the EPSI readout simultaneously acquires one spatially encoded dimension (k_x) and one temporal dimension (t_2), we propose the use of NUS in the remaining k_y–t_1 plane, followed by compressed sensing reconstruction (MaxEnt and TV). A 4 × NUS was imposed along the plane containing the incremented spectral and spatial dimensions (t_1 and k_y). Despite the mixing of spatial and spectral dimensions in the reconstruction, the sparsity requirement for reconstruction is shown to be satisfied, as required by compressed sensing. As the k_y–t_1 values are incremented, NUS can be applied along the k_y–t_1 plane.

The individual voxel volume in human prostate was 1 mL. Two sets of data were collected: one water-suppressed (WS) scan with a total scan time of 12 min and a second non-water-suppressed (NWS) scan using one average and one t_1 increment (30 s). The NWS scan was used for phase corrections (eddy current corrections). The full width at half-maximum of the water peak in the cancerous and non-cancerous locations was between 20 and 25 Hz.

Data analysis

The NUS data were reconstructed by MaxEnt and TV separately. A modified Split–Bregman algorithm (28) solves the unconstrained TV optimization problem as:

$$\min_{m} \|\nabla_m\|_1 + \lambda \|F_u m - y\|_2 \quad [1]$$

where ∇ is the gradient operator, m is the reconstructed data, $\|x\|_1$ is the l_1-norm, λ is a regularization parameter, F_u is the

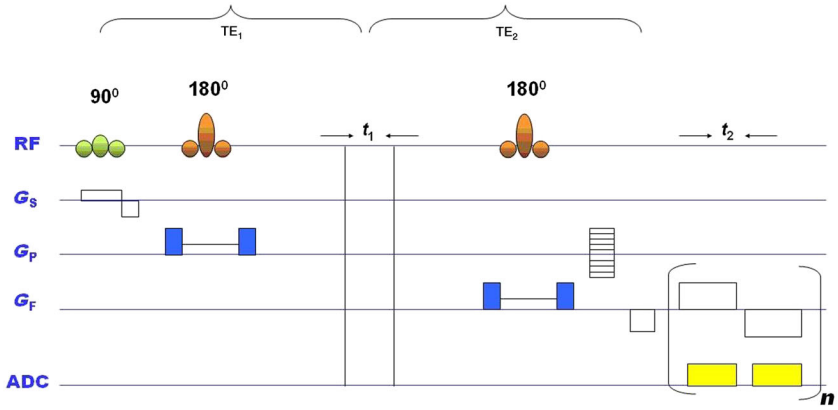

Figure 1. Schematic diagram of the four-dimensional (4D) echo planar *J*-resolved spectroscopic imaging (EP-JRESI) pulse sequence with the volume of interest (VOI) localized using point-resolved spectroscopy with three radiofrequency (RF) pulses (90°, 180°, 180°). The indirect dimension (t_1) was introduced before the last 180° pulse. ADC, analog to digital converter; G_S, G_P and G_F, gradients for slice selection, phase encoding and frequency encoding, respectively; t_2, detected dimension; *n*, number of echo planar imaging bipolar readouts.

undersampled Fourier transform and *y* is the undersampled data. The above equation removes the incoherent artifacts caused by NUS by minimizing TV, whilst maintaining consistency with the sampled measurements. The TV regularization parameters were the same as reported by Burns *et al.* (29). We have used the Split–Bregman reconstruction method primarily for its robustness against the regularization parameters chosen. Because of the use of Bregman parameters in the reconstruction algorithm, which are calculated using the difference between the reconstruction and the sampled data at each iteration, the influence of the regularization parameters is greatly lessened compared with the use of other algorithms that solve the TV problems. Although the choice of parameters can influence the reconstruction, the algorithm allows for a wider range of possible values in order to achieve roughly the same results.

MaxEnt is a constrained convex optimization algorithm that uses a variant of the conjugate gradient method to iteratively solve the inverse problem (23,25,28):

$$\text{maximize } S_{1/2}(f) \text{ such that } \left\| F^{-1} Kf - D \right\|_2 \leq \sigma \qquad [2]$$

where *f* is the estimated fully sampled spectrum at each iteration, F^{-1} is the inverse Fourier transform, *K* is the NUS matrix, *D* is the measured time domain data, σ is the noise standard deviation and $S_{1/2}(f)$ is the spin – ½ entropy of the estimated spectrum (24). All compressed sensing 4D EP-JRESI data were processed using TV and MaxEnt reconstruction with custom MATLAB software. The reconstruction time for each method took about 25 min using an 8 GB RAM, Intel Core i7-2600 CPU @ 3.40 GHz. For the 2D data processing, the raw matrix was apodized with phase shifted and squared sine bell functions along t_1 and t_2, and zero filled to 128 × 1024 prior to fast Fourier transformation along the two dimensions. All 2D spectra were presented as contour plots, and the 2D spectral matrices were not skewed by 45° about F_1 = 0 Hz.

Statistical analysis

Statistical analyses were performed with SPSS 21 (SPSS Inc., Chicago, IL, USA). Using logistic regression analysis, areas under the curve (AUCs) of the receiver operating characteristic (ROC) were calculated for various metabolites to discriminate between MaxEnt and TV reconstruction methods. In addition, the paired *t*-test was used to determine the various metabolite ratios in cancerous and non-cancerous locations. $p < 0.05$ was considered to be statistically significant.

RESULTS

Using this pilot validation, 2D peaks attributed to Cit, Ch, Cr, Spm, myo-inositol (mI) and glutamate (Glu) plus glutamine (Gln) (Glu + Gln = Glx) were quantified in cancerous and non-cancerous locations using the peak integration MATLAB code. Figure 2 shows (Ch + Cr)/Cit, (Ch + Cr)/Spm, (Ch + Cr)/mI and (Ch + Cr)/Glx of cancerous and non-cancerous locations processed by TV and MaxEnt. The mean metabolite ratios (± standard deviation, SD) of Cit, Spm, mI and Glx of the non-cancerous locations, processed using TV, were 1.158 ± 0.830, 2.396 ± 1.95, 5.325 ± 2.42 and 5.404 ± 2.74, respectively. In the cancerous locations, the corresponding metabolite ratios were: 4.209 ± 2.132, 2.808 ± 1.77, 5.640 ± 2.18 and 5.275 ± 2.80. Similarly, the mean metabolite ratios (±SD) of Cit, Spm, mI and Glx of the non-cancerous locations, calculated using the MaxEnt-reconstructed data, were 1.079 ± 0.795, 2.096 ± 1.06, 4.967 ± 2.114 and 5.902 ± 3.40, respectively. In the cancerous locations, the corresponding metabolite ratios were 3.620 ± 1.759, 2.727 ± 1.46, 6.008 ± 2.57 and 5.275 ± 3.19.

We found that the mean Cit metabolite ratios were significantly higher in cancerous locations relative to non-cancerous locations in both the TV and MaxEnt reconstructions ($p < 0.005$). Increased levels of Spm ($p = 0.46$) and mI ($p = 0.65$) ratios, and decreased levels of Glx ($p = 0.88$) ratios, were observed in cancerous locations relative to non-cancerous locations in the TV reconstruction. Similarly, in the MaxEnt reconstruction, increased levels of Spm ($p = 0.25$) and mI ($p = 0.15$) ratios, and decreased levels of Glx ($p = 0.81$) ratios, were observed in cancerous locations relative to non-cancerous locations. None of the ratios could discriminate significantly between differing grades (Gleason scores) of PCa because of overlap of the ratio values.

Figure 3 shows spatial maps of (Ch + Cr) for the TV and MaxEnt reconstructed data acquired in a 74-year-old patient with PCa. The MaxEnt and TV reconstructions of the cancerous (Fig. 4B, D) and non-cancerous (Fig. 4C, E) locations extracted from the

NMR IN BIOMEDICINE

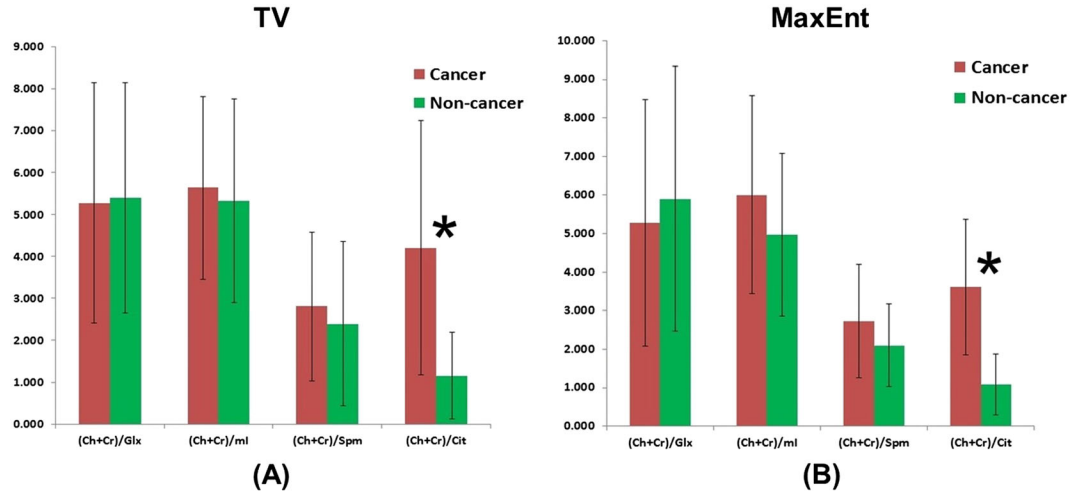

Figure 2. Metabolite ratios of citrate (Cit), spermine (Spm), myo-inositol (mI) and glutamine + glutamate (Glx) in cancerous and non-cancerous locations processed by non-linear reconstruction methods using total variation (TV) and maximum entropy (MaxEnt). Ch, choline; Cr, creatine.

JPRESS spectrum, obtained from the 4D EP-JRESI data, are shown in Fig. 4. Figure 4C illustrates the regions of interest used for peak integration. We compared and correlated the TV and MaxEnt reconstruction methods for Cit, Spm, mI and Glx in the cancerous and non-cancerous locations. The correlation of the (Ch + Cr)/Cit, (Ch + Cr)/Spm, (Ch + Cr)/mI and (Ch + Cr)/Glx ratios for the MaxEnt and TV reconstructions in the cancerous locations are shown in Fig. 5. For each patient, two to three voxels were selected in the PZ of the cancerous and non-cancerous locations, and the average values for each location were reported. A positive correlation was found for the following metabolites in the cancerous locations: (Ch + Cr)/Cit (R^2 = 0.85), (Ch + Cr)/Glx (R^2 = 0.96), (Ch + Cr)/Spm (R^2 = 0.86) and (Ch + Cr)/mI (R^2 = 0.95). The concentration of Cit is higher in healthy prostate. Hence, if the Cit peak was higher than the Ch peak, the voxel was considered to be non-cancerous for (Ch + Cr)/Cit values below 0.5 and malignant for (Ch + Cr)/Cit values above 0.5. These values were selected manually on each subject.

The results of the logistic regression analysis and consequent ROC curve analyses are given in Table 1, including the sensitivity, specificity, positive predictive value (PPV), negative predictive value (NPV), AUC and accuracy for the classification of the MaxEnt and TV methods. ROC curve analyses for differentiating the metabolite ratios of cancerous and non-cancerous locations in MaxEnt suggest that the Cit ratio gives the best predictability, with a sensitivity of 86.4%, specificity of 90.0%, accuracy of 88.6% and AUC = 94.0%. In addition, the overall sensitivity, specificity, accuracy and AUC of mI and Spm were slightly better in MaxEnt compared with TV.

DISCUSSION

Using the NUS data with non-linear iterative reconstruction, we have validated the TV and MaxEnt reconstruction methods independently in patients with PCa using EP-JRESI in a clinically feasible time. In addition to a significantly increased Cit ratio in cancerous locations, increased metabolite ratios of Spm and mI, and decreased ratios of Glx, were found in cancerous locations compared with non-cancerous locations. Although TV and

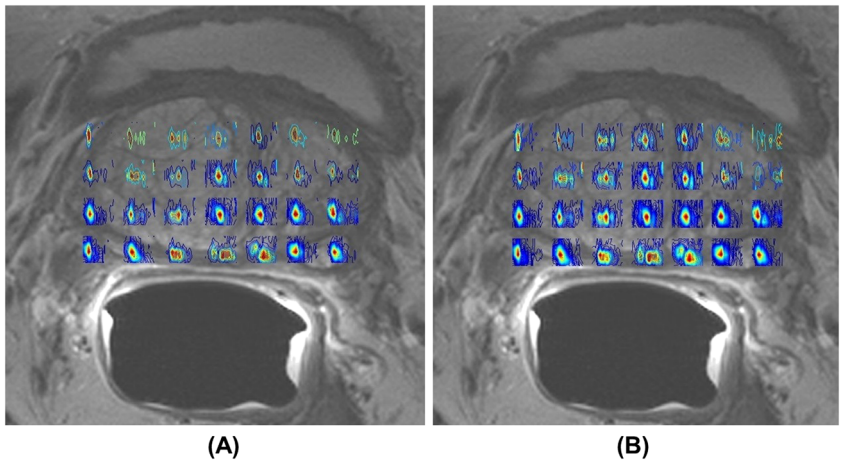

Figure 3. Spatial maps of (choline + creatine) [(Ch + Cr)] for total variation (TV) (A) and maximum entropy (MaxEnt) (B) non-linear reconstruction methods of the four-dimensional (4D) echo planar *J*-resolved spectroscopic imaging (EP-JRESI) data recorded in a 74-year-old patient with prostate cancer (PCa). EP-JRESI was overlaid on top of the T_2-weighted MRI.

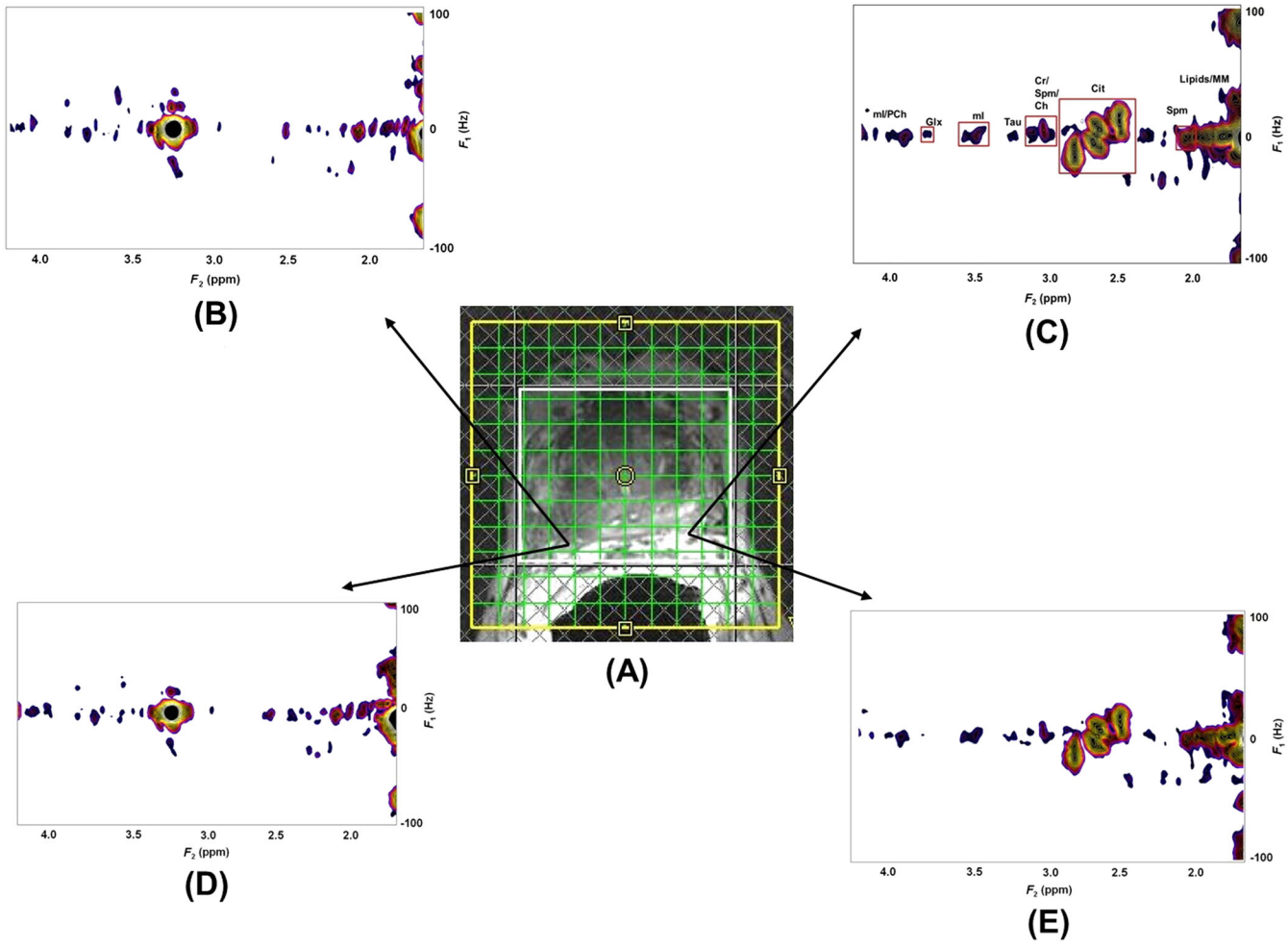

Figure 4. Echo planar *J*-resolved spectroscopic imaging (EP-JRESI) voxel localization on top of the T_2-weighted MRI (A); two-dimensional (2D) *J*-resolved spectroscopy (JPRESS) spectra extracted from the maximum entropy (MaxEnt) and total variation (TV) reconstructions of cancerous (B, D) and non-cancerous (C, E) locations. The regions of interest used for peak integration are shown in (C); (MM, macromolecules; Cit, citrate; Glx, glutamine + glutamate; mI/PCh, myo-inositol/phosphocholine; Tau, taurine; Spm, spermine).

MaxEnt reconstruction methods showed comparable results in cancerous and non-cancerous locations, the sensitivity, accuracy and AUC were slightly increased in the MaxEnt reconstruction.

In the present study, we report the ratios of (Ch + Cr)/Cit, (Ch + Cr)/Spm, (Ch + Cr)/mI and (Ch + Cr)/Glx, because of the proximity of the total Cr peak (3.0 ppm) to the total Ch peak (3.2 ppm) in these *in vivo* MR spectra, which were therefore not always separable. In this study, significantly higher ratios of Cit were observed in the PZ of cancerous locations.

It is likely that the drop in Cit levels precedes malignant transformation (30). It has been suggested that, as a result of a metabolic switch, neoplastic cells oxidize Cit, whereas normal prostatic cells show a low Cit oxidizing capability (31). Decreased levels of zinc, which would relieve *m*-aconitase from inhibition, has been proposed as one of the reasons for the decreased level of Cit in PCa (30).

Ch is an essential component of cell membrane synthesis and phospholipid metabolism, and functions as an important methyl donor. Ch-containing molecules are an essential component of cell membranes, which are more highly concentrated in tumorous areas within the prostate than in healthy prostate tissue (32,33). Ch groups are precursors and breakdown products of the phospholipid phosphatidylcholine, a major cell membrane compound (34). Increased Ch is observed as a result of altered phospholipid metabolism in PCa cell lines (33). This alteration is most probably a result of an increased expression and activity of choline kinase, a higher rate of Ch transport and an increased phospholipase activity (34).

The polyamines Spm, spermidine and putrescine are essential for the differentiation and proliferation of cells, the synthesis of DNA, RNA and proteins, and the stabilization of cell membranes and cytoskeletal structures (35). Previous studies have observed high levels of Spm in healthy prostate tissue and benign prostatic hyperplasia, and reduced Spm levels in malignant prostate tissue (16,36–38).

The osmoregulator mI is expressed in a variety of tissues, and its decrease was observed in PCa within human expressed prostatic secretions using high-resolution NMR (39) and in breast tumors (40). In our study, slightly increased mI ratios were observed in cancerous locations, but were not statistically significant.

Glu and Gln are difficult to resolve owing to resonance overlap. As a result, most MRS studies use the sum of Glu and Gln (expressed as Glx or Glu + Gln). Glu is extensively involved in metabolic and oncogenic pathways. Koochekpour (41) showed that serum Glu levels correlated directly with Gleason scores

NMR IN BIOMEDICINE

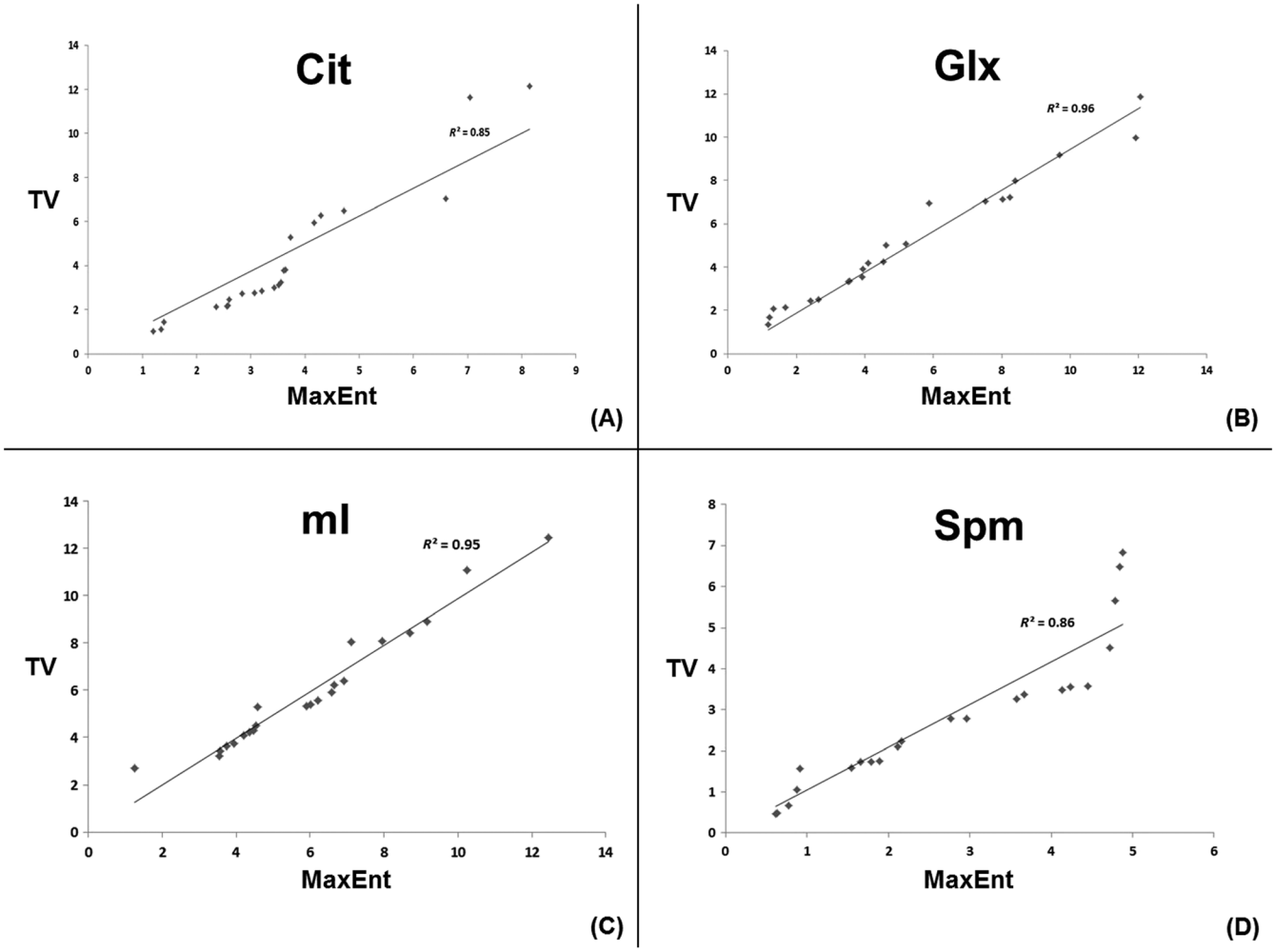

Figure 5. Correlation of maximum entropy (MaxEnt) and total variation (TV) non-linear reconstruction methods for citrate (Cit) (A), glutamine + glutamate (Glx) (B), myo-inositol (mI) (C) and spermine (Spm) (D) in cancerous locations. R^2 values are shown for each metabolite.

Table 1. Measures of sensitivity, specificity, positive predictive value (PPV), negative predictive value (NPV) and accuracy of maximum entropy (MaxEnt) and total variation (TV) methods using receiver operating characteristic (ROC) curve analysis

Metabolite	Sensitivity (%)	Specificity (%)	Accuracy (%)	PPV (%)	NPV (%)	AUC (%)
MaxEnt						
Cit	86.4	90.0	88.6	90.5	87.0	94.0
Glx	66.6	31.8	47.7	48.3	46.7	56.9
mI	54.5	63.6	59.1	60.0	58.3	65.1
Spm	50.0	72.7	61.4	64.7	59.3	64.9
TV						
Cit	86.4	90.9	88.6	90.5	87.0	92.1
Glx	63.6	36.4	50.0	50.0	50.0	57.2
mI	40.9	59.1	50.0	50.0	50.0	58.5
Spm	50.0	63.6	56.8	57.9	56.0	58.5

Cit, citrate; Glx, glutamine + glutamate; mI, myo-inositol; Spm, spermine.

(<6 *versus* >8) and primary PCa aggressiveness. In our study, decreased Glx ratios were found in cancerous locations, but were not statistically significant.

There was an overlap between cancerous and non-cancerous locations, possibly as a result of the low SNR of the Cr peak. As a result of patient movement and B_0 inhomogeneity, the resonances of Ch, Cr and Spm are difficult to resolve, especially in cancerous locations, adding to the uncertainty in quantification. However, the use of prior knowledge fitting (ProFit) may improve accurate metabolite (42) quantification, which warrants future

investigation. As a result of the limited patient population, we did not find any significant changes in other metabolites. In addition, this study focused on the PZ of the prostate, where only 80% of cancer occurs. The advantage of the compressed sensing-based 4D EP-JRESI sequence is that it records short TE-based spectra from multiple regions of human prostate, and additional metabolites, such as ml, Spm and Glx, to the normally detected Cit, Cr and Ch.

This pilot work demonstrated the use of slice-based 4D EP-JRESI, and future work will focus on volume-based, five-dimensional (5D) EP-JRESI in PCa (43). Compressed sensing-based 4D EP-JRESI shortens the total acquisition time, effectively enabling future potential to extend to pathological evaluations in a clinical set-up. The current validation method may require further optimization to improve the overall performance. As reported by Burns *et al*. (26), the sample mask is crucial to the SNR of each reconstructed prostate metabolite for the 4D EP-JRESI data. Further optimization of the reduction in non-linearity of the reconstructed peaks may enable accurate quantification of metabolites. In addition, future work will address the use of Poisson gap *versus* deterministic sample masks, and the optimization of the modulation functions for specific metabolites relevant to PCa.

CONCLUSION

We were able to detect metabolites in PCa using compressed sensing-based 4D EP-JRESI data acquired in clinically acceptable times (<12 min). We have shown that it is possible to undersample the 4D EP-JRESI sequence with an acceleration factor of four times, and that the data can be reliably reconstructed using the TV and MaxEnt methods. Both non-linear reconstruction methods provided comparable results.

Acknowledgements

This work was supported by a Congressionally Directed Medical Research Program (CDMRP) grant from the US Army Prostate Cancer Research Program (#W81XWH-11-1-0248) and National Institutes of Health / National Cancer Institute (NIH/NCI) (P50CA092131).

REFERENCES

1. Siegel R, Naishadham D, Jemal A. Cancer statistics, 2013. CA Cancer J. Clin. 2013; 63(1): 11–30.
2. Andriole GL, Crawford ED, Grubb RL 3rd, Buys SS, Chia D, Church TR, Fouad MN, Gelmann EP, Kvale PA, Reding DJ, Weissfeld JL, Yokochi LA, O'Brien B, Clapp JD, Rathmell JM, Riley TL, Hayes RB, Kramer BS, Izmirlian G, Miller AB, Pinsky PF, Prorok PC, Gohagan JK, Berg CD, PLCO Project Team. Mortality results from a randomized prostate-cancer screening trial. N. Engl. J. Med. 2009; 360(13): 1310–1319.
3. Smith DS, Humphrey PA, Catalona WJ. The early detection of prostate carcinoma with prostate specific antigen: the Washington University experience. Cancer 1997; 80: 1852–1856.
4. Djavan B, Ravery V, Zlotta A, Dobronski P, Dobrovits M, Fakhari M, Seitz C, Susani M, Borkowski A, Boccon-Gibod L, Schulman CC, Marberger M. Prospective evaluation of prostate cancer detected on biopsies 1, 2, 3 and 4: when should we stop? J. Urol. 2001; 166: 1679–1683.
5. McNeal JE, Redwine EA, Freiha FS, Stamey TA. Zonal distribution of prostatic adenocarcinoma. Correlation with histologic pattern and direction of spread Am. J. Surg. Pathol 1988; 12; 897–906.
6. Thomas MA, Narayan P, Kurhanewicz J, Jajodia P, Weiner MW. ^{1}H MR spectroscopy of normal and malignant human prostates in vivo. J. Magn. Reson. B 1990; 87: 610–619.
7. Kurhanewicz J, Vigneron DB, Nelson SJ, Hricak H, MacDonald JM, Konety B, Narayan P. Citrate as an in vivo marker to discriminate prostate cancer from benign prostatic hyperplasia and normal prostate peripheral zone: detection via localized proton spectroscopy. Urology 1995; 45: 459–466.
8. Kurhanewicz J, Vigneron DB, Hricak H, Narayan P, Carroll P, Nelson SJ. Three-dimensional H-1 MR spectroscopic imaging of the in situ human prostate with high (0.24–0.7-cm^{3}) spatial resolution. Radiology 1996; 198: 795–805.
9. Mansfield P. Spatial mapping of the chemical shift in NMR. Magn. Reson. Med. 1984; 1: 370–386.
10. Matsui S, Sekihara K, Kohno H. High-speed spatially resolved high-resolution NMR spectroscopy. J. Am. Chem. Soc. 1985; 107: 2817–2818.
11. Posse S, Tedeschi G, Risinger R, Ogg R, Bihan DL. High speed ^{1}H spectroscopic imaging in human brain by echo planar spatial–spectral encoding. Magn. Reson. Med. 1995; 33: 34–40.
12. Ericsson A, Weis J, Sperber GO, Hemmingsson A. Measurements of magnetic field variations in the human brain using a 3D-FT multiple gradient echo technique. Magn. Reson. Med. 1995; 33: 171–177.
13. Ebel A, Soher BJ, Maudsley AA. Assessment of 3D proton MR echo-planar spectroscopic imaging using automated spectral analysis. Magn. Reson. Med. 2001; 46: 1072–1078.
14. Du W, Du YP, Fan X, Zamora MA, Karczmar GS. Reduction of spectral ghost artifacts in high-resolution echo-planar spectroscopic imaging of water and fat resonances. Magn. Reson. Med. 2003; 49(6): 1113–1120.
15. Ryner LN, Sorenson JA, Thomas MA. Localized 2D J-resolved ^{1}H MR spectroscopy: strong coupling effects in vitro and in vivo. Magn. Reson. Imaging 1995; 13(6): 853–869.
16. Nagarajan R, Gomez AM, Raman SS, Margolis DJ, McClure T, Thomas MA. Correlation of endorectal 2D JPRESS findings with pathological Gleason scores in prostate cancer patients. NMR Biomed. 2010; 23(3): 257–261.
17. Lustig M, Donoho D, Pauly JM. Sparse MRI: the application of compressed sensing for rapid MR imaging. Magn. Reson. Med. 2007; 58(6): 1182–1195.
18. Hu S, Lustig M, Balakrishnan A, Larson PE, Bok R, Kurhanewicz J, Nelson SJ, Goga A, Pauly JM, Vigneron DB. 3D compressed sensing for highly accelerated hyperpolarized (13)C MRSI with in vivo applications to transgenic mouse models of cancer. Magn. Reson. Med. 2010; 63(2): 312–321.
19. Geethanath S, Baek HM, Ganji SK, Ding Y, Maher EA, Sims RD, Choi C, Lewis MA, Kodibagkar VD. Compressive sensing could accelerate ^{1}H MR metabolic imaging in the clinic. Radiology 2012; 262(3): 985–994.
20. Cao P, Wu EX. Accelerating phase-encoded proton MR spectroscopic imaging by compressed sensing. J. Magn. Reson. Imaging 2015; 41(2): 487–495.
21. Furuyama JK, Wilson NE, Burns BL, Nagarajan R, Margolis DJ, Thomas MA. Application of compressed sensing to multidimensional spectroscopic imaging in human prostate. Magn. Reson. Med. 2012; 67(6): 1499–1505.
22. Sarma MK, Nagarajan R, Macey PM. Accelerated echo-planar J-resolved spectroscopic imaging in the human brain using compressed sensing: a pilot validation in obstructive sleep apnea. Am. J. Neuroradiol. 2014; 35(6 Suppl): S81–S89.
23. Skilling J, Bryan RK. Maximum entropy image reconstruction: general algorithm. Monthly Notices R. Astronom. Soc. 1984; 211(1): 111–124.
24. Daniell GJ, Hore PJ. Maximum entropy and NMR–a new approach. J. Magn. Reson. 1989; 4(3): 515–536.
25. Hoch J, Stern AS. *NMR Data Processing*. Wiley: New York, NY; 1996.
26. Burns B, Wilson NE, Furuyama JK, Thomas MA. Non-uniformly under-sampled multi-dimensional spectroscopic imaging in vivo: maximum entropy versus compressed sensing reconstruction. NMR Biomed. 2014; 27(2): 191–201.
27. Rudin L, Osher S, Fatemi E. Nonlinear total variation based noise removal algorithms. Physica D 1992, 60: 259–268.
28. Goldstein T, Osher S. The Split Bregman method for L1 regularized problems. SIAM J. Imaging Sci. 2009; 2: 323–343.
29. Burns BL, Wilson NE, Thomas MA. Group sparse reconstruction of multi-dimensional spectroscopic imaging in human brain in vivo. Algorithms 2014; 7(3): 276–294.
30. Costello LC, Franklin RB. The intermediary metabolism of the prostate: a key to understanding the pathogenesis and progression of prostate malignancy. Oncology 2000; 59: 269–282.
31. Costello LC, Franklin RB, Narayan P. Citrate in the diagnosis of prostate cancer. Prostate 1999; 38: 237–245.

32. Kurhanewicz J, Swanson MG, Nelson SJ, Vigneron DB. Combined magnetic resonance imaging and spectroscopic imaging approach to molecular imaging of prostate cancer. J. Magn. Reson. Imaging 2002; 16(4): 451–463.
33. Ackerstaff E, Pflug BR, Nelson JB, Bhujwalla ZM. Detection of increased choline compounds with proton nuclear magnetic resonance spectroscopy subsequent to malignant transformation of human prostatic epithelial cells. Cancer Res. 2001; 61: 3599–3603.
34. Glunde K, Bhujwalla ZM. Metabolic tumor imaging using magnetic resonance spectroscopy. Semin. Oncol. 2011; 38: 26–41.
35. Jänne J, Pösö H, Raina A. Polyamines in rapid growth and cancer. Biochim. Biophys. Acta 1978; 473: 241–293.
36. Van der Graaf M, Schipper RG, Oosterhof GO, Schalken JA, Verhofstad AA, Heerschap A. Proton MR spectroscopy of prostatic tissue focused on the detection of spermine, a possible biomarker of malignant behavior in prostate cancer. MAGMA 2000; 10: 153–159.
37. Thomas MA, Nagarajan R, Huda A, Margolis D, Sarma MK, Sheng K, Reiter RE, Raman SS. Multidimensional MR spectroscopic imaging of prostate cancer in vivo. NMR Biomed. 2014; 27(1): 53–66.
38. Yue K, Marumoto A, Binesh N, Thomas MA. 2D JPRESS of human prostates using an endorectal receiver coil. Magn. Reson. Med. 2002; 47(6): 1059–1064.
39. Serkova NJ, Gamito EJ, Jones RH, O'Donnell C, Brown JL, Green S, Sullivan H, Hedlund T, Crawford ED. The metabolites citrate, myo-inositol, and spermine are potential age-independent markers of prostate cancer in human expressed prostatic secretions. Prostate 2008; 68(6): 620–628.
40. Griffin JL, Shockcor JP. Metabolic profiles of cancer cells. Nat. Rev. Cancer 2004; 4: 551–561.
41. Koochekpour S. Glutamate, a metabolic biomarker of aggressiveness and potential therapeutic target for prostate cancer. Asian J. Androl. 2013; 15(2): 212–213.
42. Lange T, Schulte RF, Boesiger P. Quantitative J-resolved prostate spectroscopy using two-dimensional prior-knowledge fitting. Magn. Reson. Med. 2008; 59(5): 966–972.
43. Wilson NE, Iqbal Z, Burns BL, Keller M, Thomas MA. Accelerated five-dimensional echo planar J-resolved spectroscopic imaging: implementation and pilot validation in human brain. Magn. Reson. Med. 2015. doi: 10.1002/mrm.25605. [Epub ahead of print]

Semi-Laser 5D Echo-Planar J-Resolved Spectroscopic Imaging: Pilot validation in Prostate Cancer

Zohaib Iqbal[1], Neil E. Wilson[1], Rajakumar Nagarajan[1], Daniel A. Margolis[1], Robert E. Reiter[2], Steven S. Raman[1], and Michael Albert Thomas[1]

[1]*Radiological Sciences, University of California - Los Angeles, Los Angeles, California, United States,* [2]*Urology, University of California - Los Angeles, Los Angeles, California, United States*

Target Audience: Basic scientists interested in Compressed Sensing (CS) reconstruction of semi-laser based multi-dimensional spectroscopic imaging (3 spatial and 2 spectral dimensions), as well as clinicians interested in spectroscopic imaging of in vivo prostate.

Purpose: Alongside lung cancer, prostate cancer is one of the leading causes of cancer death in men [1]. J-resolved spectroscopy (JPRESS) is a technique that utilizes a two-dimensional (2D) acquisition to spread overlapping resonances into a second spectral dimension, and has shown to be useful in assessing severity of prostate cancer [2, 3]. Spectroscopic imaging of this technique provides greater spatial coverage [4], however in order to acquire data in a clinically feasible time, an echo-planar readout becomes a necessity to acquire one spatial and one spectral domain simultaneously [5]. In order to further reduce scan time, a non-uniform undersampling (NUS) scheme can be applied to the incremented dimensions, and the resulting data can be reconstructed using CS reconstruction [6]. Due to the limited bandwidth of classical 180º pulses, chemical shift displacement error (CSDE) is apparent. Using a pair of adiabatic 180º pulses to replace these smaller bandwidth pulses has shown to limit CSDE [7]. The purpose of this study was to develop a 5 dimensional (5D) technique (3 spatial and 2 spectral dimensions) capable of covering the entire prostate utilizing an echo-planar readout, a NUS scheme on the (k_y,k_z,t_1) dimensions with CS reconstruction, and semi-Laser pulses to reduce CSDE. This sequence, called semi-Laser 5D echo-planar J-resolved Spectroscopic Imaging (5D EP-JRESI), was used to investigate the prostate for healthy volunteers and prostate cancer patients.

Methods: A semi-Laser 5D EP-JRESI sequence with a maximum echo sampling scheme was developed and used to scan four healthy volunteers (mean age = 54.5 years old) and two prostate cancer patients (mean age= 54 years old) using a multi-channel body array coil for healthy or a single channel endorectal coil for patients. For the semi-laser based sequence, the overall structure was similar to the 5D EP-JRESI sequence [8], however each 180º pulse was replaced with a pair of 180º adiabatic pulses [7]. The t_1 increment was placed in between the two pairs of adiabatic pulses. The pulse sequence diagram can be seen in Figure 1. The following parameters were used for data acquisition: TE=41 ms, TR=1000 ms, spectral bandwidth=1190/1000 Hz, number of t_2 points = 256, number of t_1 points = 64, FOV = 16x16x12 cm^3, and resolution = 1x1x1.5 cm^3, and the total scan time was approximately 17 minutes. The echo planar readout was used to simultaneously acquire 32 (oversampled) k_x points and 256 t_2 points, and the other spatial dimensions were acquired using 16 points for k_y and 8 points for k_z. A NUS scheme was applied to achieve an acceleration factor of 8x. Before the data were reconstructed, the data were truncated to only include the spectral region of interest (F_2 = 1.2-4.3 ppm) in order to ensure minimal water contamination. The data was reconstructed using a modified split Bregman algorithm that minimizes total variation (TV) [6]. Select voxels from healthy and unhealthy regions in the prostate, as determined from biopsy, were qualitatively assessed.

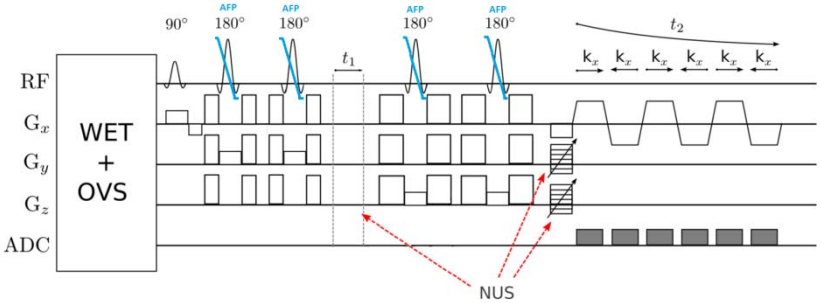

Figure 1. The pulse sequence diagram for semi-Laser 5D NUS Echo-Planar J-resolved Spectroscopic Imaging (5D EP-JRESI).

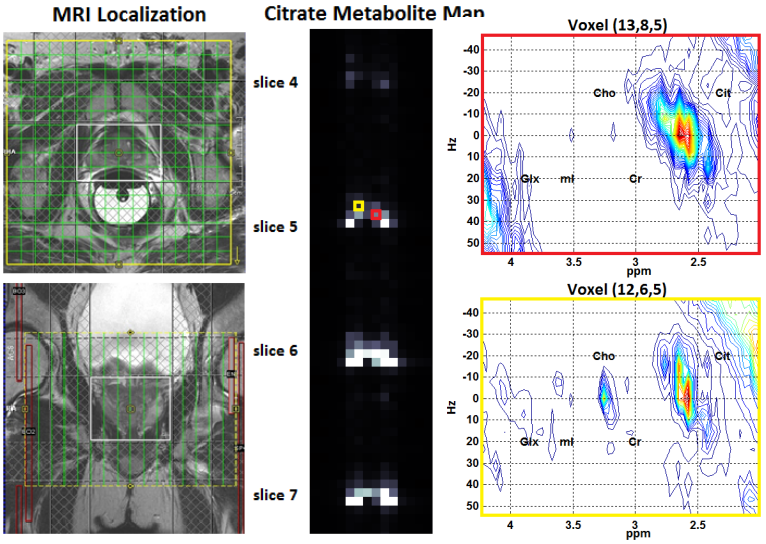

Figure 2. MRI localization (left) of axial (top) and coronal (bottom) views of a cancer patient's (age = 51 years old) prostate are shown. A citrate metabolite map (middle) shows signal from three different slices. Two spectra (right) are shown corresponding to the colors on the citrate metabolite map. Red is the healthy region, determined from the biopsy, and yellow is the unhealthy region.

Results: Qualitative analysis of the 2D spectra from the 51 year old cancer patient, displayed on the right in Figure 2, shows that lower citrate and higher choline are present in the voxel that corresponds to the unhealthy region of the prostate (as determined from a biopsy).

Discussion: The results show that for this patient, healthy and unhealthy prostate regions could be differentiated based on the 2D spectra. However, due to motion during the scan, several voxels contained severe lipid contamination (hyper-intense regions on the citrate metabolite map). This contamination may be minimized by using an inversion pulse for lipid suppression [9], and will be implemented in the future.

Conclusion: Semi-Laser 5D EP-JRESI has been implemented in healthy volunteers and prostate cancer patients, and is capable of full prostate coverage. Future work will focus on recruiting more healthy volunteers and patients, quantifying the 2D spectra using prior knowledge fitting, and further optimizing the sequence to avoid lipid contamination.

Acknowledgements: US Army Prostate Cancer Research Program: (#W81XWH-11-1-0248).

References: [1] American Cancer Society. Cancer Facts & Figures 2013. *Atlanta Georgia: American Cancer Society 2013.* [2] Ryner LN, Sorenson JA, Thomas MA. *Magn Reson Imaging* 1995;6:853-869. [3] Nagarajan R, Gomez AM, Raman SS, et al. *NMR Biomed* 2010;23:257-261. [4] Lipnick S, Verma G, Ramadan S, et al. *Magn Reson Med* 2010;64:947-956. [5] Posse S, DeCarli C, Le Bihan D. *Radiology* 1994;192:733-8. [6] Furuyama JK, Wilson NE, Burns BL, et al. *Magn Reson Med* 2012;67:1499-1505. [7] Lin M, Kumar A, Yang S. *Magn Reson Med* 2014;71:911-920. [8] Wilson NE, Iqbal Z, Burns BL, et al. *22nd ISMRM meeting* 2014; #0481. [9] Spielman DM, Pauly JM, Macovski A, et al. *J Magn Reson* 1992;2:253-262.

×

PHE118

Close

PHE118

Education Exhibits

How Accurately Multiparametric MRI Detect Prostate Cancer?

Thursday, 12:15 - 12:45 PM
Location: PH Community, Learning Center
Station #8

PARTICIPANTS:

Rajakumar Nagarajan PhD **(Presenter)**: Nothing to Disclose
Daniel J Margolis MD: Research Grant, Siemens AG
Steven S Raman MD: Consultant, Bayer AG Consultant, Covidien AG
Michael A Thomas PhD: Nothing to Disclose

CITE THIS ABSTRACT

Nagarajan,R, Margolis,D, Raman,S, Thomas,M, How Accurately Multiparametric MRI Detect Prostate Cancer?. Radiological Society of North America 2014 Scientific Assembly and Annual Meeting, November 30 - December 5, 2014, Chicago IL. rsna2014.rsna.org/program/details/?emID=14007386 Accessed December 10, 2014

TEACHING POINTS

Multiparametric magnetic resonance imaging techniques are increasingly being used to address bottlenecks in prostate cancer patient management. These techniques yield qualitative, semi-quantitative and fully quantitative biomarkers that reflect on the underlying biological status of a tumor. 1. Teach the concept of prostate MRI and MRSI. 2. Demonstrate the importance of functional and anatomic information in prostate. 3. Show clinical applications that benefit from multiparametric MRI. 4. This functional and anatomical MRI and MRSI guide urologists and radiotherapists so that they may be used for individual patient decision making.

TABLE OF CONTENTS/OUTLINE

CONTENT ORGANIZATION 1. Introduction of T2 Weighted MRI (T2W), Diffusion weighted imaging (DWI), Dynamic contrast enhanced (DCE) MRI and Magnetic Resonance Spectroscopic Imaging (MRSI) of Prostate. 2. Demonstration of MRI and MRSI sequences used in Prostate Images. 3. Data interpretation of T2W, DWI, DCE-MRI and MRSI. 4. Comparison of sensitivity, specificity, positive predictive value, negative predictive value and accuracy of each modality.